

On the net displacement of contractile elastic bodies subjected to surface friction

José J. Muñoz^{1,2}, Lucie Condamin³, David Doste⁴

¹Mathematics Department, Laboratori de Càlcul Numèric (LaCàN), Universitat Politècnica de Catalunya, Barcelona, Spain.

<http://www.lacan.upc.edu/jose.munoz>, j.munoz@upc.edu

²Centre International de Mètodes Numèrics en Enginyeria (CIMNE), Barcelona, Spain.

³Institut National des Sciences Appliquées, Lyon, France.

⁴Facultat de Matemàtiques i Estadística, Universitat Politècnica de Catalunya, Barcelona, Spain.

Abstract

We show that for an elastic body undergoing a set of self-equilibrated contractile forces and negligible inertial forces, and subjected to a linear frictional boundary condition, the mean displacement averaged on the contact surface is zero. This fact demonstrates the inability of slender organisms to move under this friction condition if the contact surface remains constant, regardless of the contractility strategy employed. We extend our results to non-homogeneous and anisotropic friction, illustrate our conclusions with two examples, and comment on strategies for net propulsion.

1 Introduction

Mechanisms for locomotion of organisms have been well studied in fluids [8, 24] and granular media [5, 28]. However, only in the former case exist general principles for propulsion, which have been mainly derived for low Reynolds number [11, 21]. When bodies are submerged in a fluid, Purcell’s scallop theorem furnishes sufficient conditions for the null net motion in fluids through the analysis of the parametric space of body configurations [20, 21]. In these results, Stokes equations are imposed, with a no-slip boundary condition.

Limbless self-propulsion of deformable solids on loose soil or granular matter has been analysed and modelled in detail [4, 12], and a theory that allows determining the propulsion from the interaction with the granular environment, so-called resistive force theory, has been derived and validated [13, 18, 12]. However, partially due to the complex interaction at the boundary, no general equivalent theorem furnishing sufficient conditions for the no net motion of the body centre (centre of mass when density is constant)

on a frictional substrate has been established. This paper aims at furnishing some results along this direction.

In order to analyse the motion on a frictional substrate, we assume an elastic body Ω with the ability to self-contract. Similar to the analysis in fluids, and due to the small size of Ω and the low accelerations, we neglect the contribution of inertial effects [15]. We will consider thin or elongated organisms, such that in this case boundary forces can be approximated by body forces applied in the body domain Ω , which is initially occupying domain Ω_0 . We will also comment the situation when the whole limbless body is permanently in contact with the frictional substrate. The lifting or removal of friction will be discussed after deriving our main results.

2 Motion of contact surface centre

More specifically, we are interested in analysing the motion of the body centre $\bar{\mathbf{x}} = \int_{\Omega} \mathbf{x} dV / V$, with vol-

ume $V = \int_{\Omega} dV$. The ability to *self-contract* is represented by a field of N dipoles with opposing forces $\mathbf{f} = \sum_i^N \pm p_i \mathbf{n}_i \delta(\mathbf{x}_i^{\pm})$ and magnitude p_i , applied at points $\mathbf{x} = \mathbf{x}_i^+$ and $\mathbf{x} = \mathbf{x}_i^-$ along directions $\pm \mathbf{n}_i = \pm(\mathbf{x}_i^+ - \mathbf{x}_i^-)/\|\mathbf{x}_i^+ - \mathbf{x}_i^-\|$, respectively. Note that the set of dipoles is indeed self-equilibrated, i.e.

$$\int_{\Omega} \mathbf{f} dV = \sum_i^N \pm p_i \mathbf{n}_i = \mathbf{0}. \quad (1)$$

We also assume that the body behaves elastically, and thus there is an elastic potential $\phi(\mathbf{u}) \geq 0$ which depends on the displacement field $\mathbf{u} = \mathbf{x} - \mathbf{x}_0$, with \mathbf{x}_0 and \mathbf{x} material points in Ω_0 and Ω . Cauchy stress tensor $\boldsymbol{\sigma}$ follows from the second Piola-Kirchhoff stress tensor $\mathbf{S} = 2 \frac{\partial \phi}{\partial \mathbf{C}}$ as $\boldsymbol{\sigma} = J^{-1} \mathbf{F} \mathbf{S} \mathbf{F}^T$, where $\mathbf{C} = \mathbf{F}^T \mathbf{F}$ is the right Cauchy-Green deformation tensor, $J = \det(\mathbf{F})$ and $\mathbf{F} = \frac{\partial \mathbf{x}}{\partial \mathbf{x}_0}$ the deformation gradient [6]. The static equilibrium of domain Ω is then given by Cauchy's equation, including the dipoles as a body force:

$$\nabla \cdot \boldsymbol{\sigma} + \mathbf{f} = \mathbf{0}, \quad \forall \mathbf{x} \in \Omega, \quad (2)$$

and with boundary conditions that we assume stemming from a frictional condition with respect to displacements

$$\boldsymbol{\sigma} \mathbf{n} = -\mu \mathbf{u}, \quad \forall \mathbf{x} \in \partial\Omega. \quad (3)$$

In the previous relation, we use a constant scalar frictional coefficient $\mu \geq 0$, although in experimental measurements with “frictional fluids” different values in the longitudinal and normal directions are commonly considered [16]. We will comment on the anisotropic and non-homogeneous cases in our discussion. As yet we mention that whether friction is proportional to displacement (dry friction) or velocities (wet friction) will not alter our conclusions, as it will be also shown later.

In the next paragraphs, we demonstrate that for slender bodies, the centre of Ω does not move, or equivalently, that the mean of the displacement vanish, i.e. $\bar{\mathbf{u}} = \int_{\Omega} (\mathbf{x} - \mathbf{x}_0) dV / V = \int_{\Omega_0} (\mathbf{x}(\mathbf{x}_0) - \mathbf{x}_0) dV_0 / V = \mathbf{0}$. For this, we first note that the associated weak form (or virtual principle) of problem in (2)-(3) follows after pre-multiplying equation (2) by a

set of compatible virtual displacements $\boldsymbol{\delta} \mathbf{u}$, integrating by parts and considering the boundary condition in (3):

Find \mathbf{u} such that, for all virtual admissible displacements $\boldsymbol{\delta} \mathbf{u}$,

$$\int_{\Omega} \boldsymbol{\varepsilon}(\boldsymbol{\delta} \mathbf{u}) : \boldsymbol{\sigma}(\mathbf{u}) dV = \pm \sum_i \boldsymbol{\delta} \mathbf{u} \cdot \mathbf{f}_i^{\pm}(\mathbf{x}_i^{\pm}) - \int_{\partial\Omega} \mu \boldsymbol{\delta} \mathbf{u} \cdot \mathbf{u} dS, \quad (4)$$

with $\boldsymbol{\varepsilon}(\boldsymbol{\delta} \mathbf{u})$ the virtual strains. The solution of the previous problem. \mathbf{u} , and also the one in (2)-(3), is in turn equivalent to finding the minimiser of a functional $W(\mathbf{u})$ given by

$$W(\mathbf{u}) = \int_{\Omega} \phi(\mathbf{u}) dV + \sum_i p_i l_i(\mathbf{u}_i) + \frac{\mu}{2} \int_{\partial\Omega} \|\mathbf{u}\|^2 dS,$$

where $l_i(\mathbf{u}_i) = \|\mathbf{x}_i^+ - \mathbf{x}_i^-\|$. Next we split the solution into its mean value and a spatial deviation from this mean, i.e. $\mathbf{u} = \bar{\mathbf{u}} + \Delta \mathbf{u}$, with $\bar{\mathbf{u}} = \int_{\Omega} \mathbf{u} dV / V$, and $\Delta \mathbf{u} = \mathbf{u} - \bar{\mathbf{u}}$. Note that by construction $\int_{\Omega} \Delta \mathbf{u} = \int_{\Omega} (\mathbf{u} - \bar{\mathbf{u}}) dV / V = \mathbf{0}$, and that $\bar{\mathbf{u}}$ is a (constant) rigid body translation. As a consequence, due to the elastic assumption, the invariance of $l_i(\mathbf{u}_i)$ with respect to translations, and that for thin or flat bodies we can set $\partial\Omega \approx \Omega$, it follows that,

$$\begin{aligned} \int_{\Omega} \boldsymbol{\varepsilon}(\mathbf{u}) : \boldsymbol{\sigma}(\mathbf{u}) dV &= \int_{\Omega} \boldsymbol{\varepsilon}(\Delta \mathbf{u}) : \boldsymbol{\sigma}(\Delta \mathbf{u}) dV \\ \sum_i p_i l_i(\mathbf{u}_i) &= \sum_i p_i l_i(\Delta \mathbf{u}_i) \\ \mu \int_{\partial\Omega} \|\mathbf{u}\|^2 dV &\approx \mu \int_{\partial\Omega} \|\Delta \mathbf{u}\|^2 dV + \mu \|\bar{\mathbf{u}}\|^2 V, \end{aligned} \quad (5)$$

which implies that,

$$W(\mathbf{u}) \approx W(\Delta \mathbf{u}) + \mu \|\bar{\mathbf{u}}\|^2 V. \quad (6)$$

Since the solution \mathbf{u} minimises $W(\mathbf{u})$, its mean value must vanish, i.e. $\bar{\mathbf{u}} = \mathbf{0}$.

We point out that the accuracy of the previous result depends on the error of the approximation $\partial\Omega \approx \Omega$. Arbitrary three-dimensional bodies are not necessarily flat or elongated, and this approximation

may be too inaccurate. In this case, (6) must be replaced by

$$W(\mathbf{u}) = W(\Delta\mathbf{u}_s) + \mu\|\bar{\mathbf{u}}_s\|^2 S, \quad (7)$$

where $\bar{\mathbf{u}}_s = \int_{\partial\Omega} \mathbf{u} dS/S$ is the mean value at the boundary $\partial\Omega$, and $\Delta\mathbf{u}_s = \mathbf{u} - \bar{\mathbf{u}}_s$. The result follows from the fact that $\int_{\partial\Omega} \Delta\mathbf{u}_s dS = \mathbf{0}$. An alternative (an shorter) procedure to reach the same result is by noting that the weak form in (4) holds for arbitrary (constant) rigid body virtual displacements $\delta\bar{\mathbf{u}}$, using the fact that $\boldsymbol{\varepsilon}(\delta\bar{\mathbf{u}}) = \mathbf{0}$, and remarking that the dipoles are self equilibrated, which yields,

$$\mu \int_{\partial\Omega} \mathbf{u} dS = \mu S \bar{\mathbf{u}}_s = \mathbf{0}. \quad (8)$$

Consequently, for general three-dimensional bodies subjected to linear homogeneous and isotropic friction, the centre of the surface in contact, \mathbf{x}_s , does not move. Diversions from such frictional condition may give rise to changes in $\bar{\mathbf{x}}_s$, like the use of different parallel and normal frictional coefficients, as employed in the resistive force theory [22, 13, 18], or resorting to different coefficients in different tangential directions, as used by euglenoids in fluids [1]. Strategies for net motion of $\bar{\mathbf{x}}$ may in turn involve the decrease or removal of friction in different regions of the boundary, like in sidewinding [4].

For general boundary friction laws with the form $\boldsymbol{\sigma}\mathbf{n} = -\boldsymbol{\mu}(\mathbf{u})$, the result in equation (8) must be replaced by,

$$\int_{\partial\Omega} \boldsymbol{\mu}(\mathbf{u}) dS = \mathbf{0}. \quad (9)$$

This type of laws include scenarios with unequal normal and tangential friction, which we will study in the second example below. We point out however that the conservation of the "weighted" displacement in (9) is though far less practical than the result for linear friction in (8).

When the boundary condition corresponds to linear wet friction [19], that is, when $\mathbf{f}^\mu = -\mu\dot{\mathbf{u}}$, similar conclusions apply, i.e. $\bar{\mathbf{u}}_s = \mathbf{0}$. Indeed, the approximation $\dot{\mathbf{u}} \approx (\mathbf{u}_{n+1} - \mathbf{u}_n)/(t_{n+1} - t_n)$ for time instants t_{n+1} and t_n allows us to write the resulting equilibrium equations as a minimisation with respect

to \mathbf{u}_{n+1} with a fixed \mathbf{u}_n , in which case we conclude that $\bar{\mathbf{u}}_{n+1} = \bar{\mathbf{u}}_n$ when $\partial\Omega \approx \Omega$, or $\bar{\mathbf{u}}_{s,n+1} = \bar{\mathbf{u}}_{s,n}$ in general three-dimensional bodies.

3 Numerical Examples

We illustrate our results with a couple of examples that will be solved numerically. The first one consists on a flat square domain $[0, L]^2$ in contact with a substrate, and contracting according to the following two strategies: a) constant friction everywhere with an applied local contractility along a thin vertical domain (see Figure 1a), and b) a contraction on the whole domain with a null friction along a thin vertical line (see Figure 1b). We test different horizontal positions c of the contracting band in case a) and different positions of the contact removal in case b). The problem is solved resorting to a finite element discretisation and the contraction is implemented by superimposing to the elastic deformation an isotropic contractile strain $\varepsilon^c \mathbf{I}$.

The numerical results confirm that in both cases the displacement of the centre of the surface with non-zero friction vanishes, i.e. $\bar{\mathbf{u}}_s = \mathbf{0}$. We show in Figure 2 the plot of $\bar{\mathbf{u}}$. In case a), since this surface also coincides with the whole body surface, we have that $\bar{\mathbf{u}} = \mathbf{0}$ for all values of c . Instead, in case b), since the centre of the surface in contact is moving backwards as c increases, the centre of the whole body $\bar{\mathbf{x}}$ moves forwards for $c < L/2$, while $\bar{\mathbf{x}}$ moves backwards for $c > L/2$. When $c = L/2$, the two centres coincide, $\bar{\mathbf{x}}_s = \bar{\mathbf{x}}$, and in this case no net displacement of the body centre is obtained, i.e. $\bar{\mathbf{u}} = \bar{\mathbf{u}}_s = \mathbf{0}$.

In a second example, we analyse a worm-like unidimensional domain that has the ability to bend and produce a wave-like undulation, similarly to the analysis presented for hydrodynamics in [26]. The worm is modelled here as a set of n planar line segments joining $n + 1$ nodes $\mathbf{x}_0, \dots, \mathbf{x}_n$. Stretching and bending elasticity is furnishing by using the following total elastic potential

$$\Phi(\mathbf{x}) = \sum_{i=0}^n k(\|\mathbf{x}_{i+1} - \mathbf{x}_i\| - l_{i0})^2 + \sum_{i=1}^n k_\theta \theta_i^2,$$

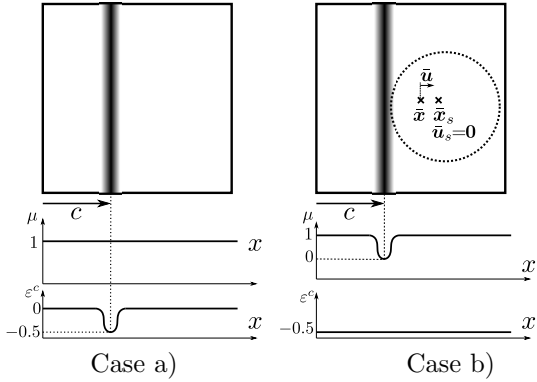


Figure 1: Example 1: Contractile square domain. a) Homogeneous friction with a localised contractility on a vertical band. b) Homogeneous contractility with a localised reduction of friction on a vertical band.

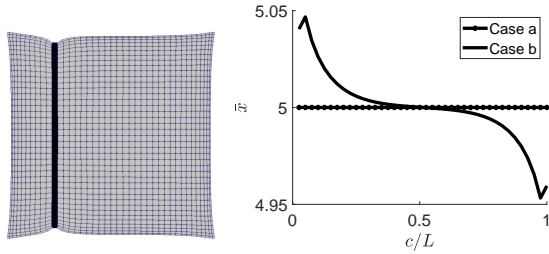


Figure 2: Example 1: Left: deformation for case b. Right: resulting displacement of motion of horizontal coordinate of the body (surface) centre.

with l_{i0} the initial length of segment $\mathbf{x}_{i+1} - \mathbf{x}_i$ and θ_i the angle between $\mathbf{x}_{i+1} - \mathbf{x}_i$ and $\mathbf{x}_i - \mathbf{x}_{i-1}$ (see Figure 3). In addition to the elastic forces, the model is subjected to nodal frictional components $\mathbf{f}_i^\mu = -\mu \mathbf{u}_i$ and a set of bending moments M_i applied at the interior nodes $i = 1, \dots, n-1$. Each bending moment M_i is in fact decomposed into three self-equilibrated forces $\mathbf{f}_i^-, \mathbf{f}_i^o, \mathbf{f}_i^+$, respectively applied at nodes $\mathbf{x}_{i-1}, \mathbf{x}_i$ and \mathbf{x}_{i+1} . These forces are normal to direction $\mathbf{x}_{i+1} - \mathbf{x}_{i-1}$, and such that $\mathbf{f}_i^- + \mathbf{f}_i^o + \mathbf{f}_i^+ = \mathbf{0}$, with a resulting bending moment equal to M_i , as also illustrated in Figure 3(left). This conditions, and the no torque resultant, defines uniquely the direction and

magnitude of the forces for a given value of M_i . The equilibrium equations for each node i read then,

$$\frac{\partial \Phi(\mathbf{x})}{\partial \mathbf{x}_i} + \mathbf{f}_i^M = \mathbf{f}_i^\mu, \quad (10)$$

where vector $\mathbf{f}_i^M = \mathbf{f}_{i-1}^+ + \mathbf{f}_i^o + \mathbf{f}_{i+1}^-$ includes all the force contributions at node i due to the contractile bending moments. We have applied a distribution of time varying moments equal to

$$M_i = \sin(\omega t - k s_i),$$

except at the end points, where $M_0 = M_n = 0$. Here, ω is the frequency, k the wave number, and s_i the initial position of point \mathbf{x}_i . Although we are not using a set of dipoles, we note that the discretised weak form of the balance equations in (10) reads,

Find $\mathbf{u}_i = \mathbf{x}_i - \mathbf{x}_{i0}$ such that for all virtual displacements $\delta \mathbf{u}_i$

$$\delta \mathbf{u} \cdot \frac{\partial \Phi(\mathbf{x})}{\partial \mathbf{x}_i} + \delta \mathbf{u} \cdot \mathbf{f}_i^M = \delta \mathbf{u} \cdot \mathbf{f}_i^\mu.$$

Since this relation must be also satisfied for arbitrary rigid body displacements, and $\sum_i \mathbf{f}_i^M = \mathbf{0}$ (forces due to applied moments are self-equilibrated by construction), we have an equivalent result to the one in (8):

$$\sum_i \mathbf{u}_i = \mathbf{0}.$$

We have numerically solved the set of n non-linear equations in (10), and verified that when isotropic friction is used, the resulting motion of the worm centre $\bar{\mathbf{x}} = \sum_i \mathbf{x}_i / n$ is exactly zero, up to machine tolerance. When the same oscillatory set of moments is used, but in conjunction with anisotropic friction $\mathbf{f}^\mu = -\mu_t \mathbf{u}_t - \mu_n \mathbf{u}_n$, with \mathbf{u}_t and \mathbf{u}_n the tangential and normal components of the displacements, and μ_t and μ_n two different friction coefficients, the worm is propelled, as shown in Figure 3 (right). In this case, the worm centre moves in the opposing direction of the wave of bending moments, as also pointed out for locomotion in fluids [8, 11] and solids [12].

We have tested different frequencies ω and wave numbers k . The sequence of horizontal displacements

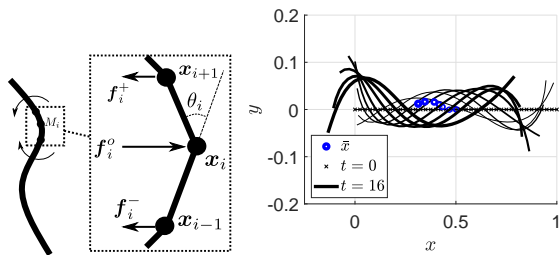


Figure 3: Example 2: Left: Worm-like domain with self-contractile moments. Right: Snapshots of deformed shape for anisotropic friction ($\mu_n = 10\mu_t = 1$).

shown in Figure 4 indicates that although final displacement increases for increasing values of ω and k , there is for both parameters a limit value beyond which no substantial improvement is observed. This fact is also confirmed by the low wave numbers and limited frequencies that organisms generally exhibit [12]. We have not focused this study on the search of optimal modes or strategies, also with respect to other motion parameters such as amplitude or friction, which have been analysed elsewhere [5, 29, 14], or simulated with the discrete element method [10]. We intend to analyse in future works more realistic resistive forces such as frictional plasticity models [2], or more complex waves such as those in sidewinding [3] or helical motion [28], and interpret them as a drift from the homogeneous frictional conditions where no motion is achieved.

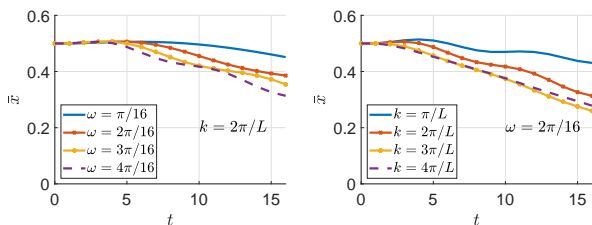


Figure 4: Example 2: horizontal displacement of the worm centre for increasing values of frequency (left) and wave number (right).

4 Discussion

The two examples presented above highlight that i) although anisotropic drag and non-time reversibility is required for locomotion in fluids [8, 20, 11], in our case, propulsion may be alternatively obtained by reducing friction on a subdomain of the body, and that ii) although we obtain a similar propulsion to the one in fluids when a contractile wave is employed, our net movement is not the result of alternating vortices [11], but should be rather interpreted as a difference between the positions of the body centre \mathbf{x} , and the average position weighted by the friction along the body boundary \mathbf{x}_s . We remark that our theoretical results are applicable to solids with non-linear constitutive laws and large displacements. However, our conclusions cannot be generalised to bodies immersed in a fluid, where a no-slip condition is assumed in this case.

We also mention that our analysis is pertinent to crawling microorganisms on frictional substrates such as *C. elegans* on agar [23, 8]. In many instances, net locomotion is achieved through the activation of contractile waves, as it is the case in lateral undulation and sidewinding, with some lifting/lowering, which results in a variation of the frictional conditions. While the measurement of the centre of mass in swimming organisms [30] and human gait dynamics [27] is common, its analysis and correlation with substrate friction at the cellular scale is usually not investigated.

Indeed, understanding sufficient conditions for the null net movement may help to elucidate the conditions for migration in cells or monolayers on substrates, where planar motion is dominant *in vitro*. For instance, substantial computational and experimental efforts have been devoted to traction force microscopy (retrieval of traction field exerted by cells or tissues) [7, 9, 17, 25]. In those cases, the motion of the tissue centre should be interpreted as a set of unequal adhesions, and not solely to differential tissue contractility. Accordingly, the configurational parametric space should be analysed jointly with modes of the contact conditions.

References

- [1] M. Arroyo, L. Heltai, D. Millan, and A. DeSimone. Reverse engineering the euglenoid movement. *Proc. Natl. Acad. Sci. USA*, 109(44):17874–17879, 2012.
- [2] H. Askari and K. Kamrin. Intrusion rheology in grains and other flowable materials. *Num. Math.*, 15:1274–1270, 2016.
- [3] H. C. Astley, C. Gong, J. Dai, M. Travers, M. M. Serrano, P. A. Vela, H. Choset, J. R. Jr. Mendelson, D. L. Hu, and D. I. Goldman. Modulation of orthogonal body waves enables high maneuverability in sidewinding locomotion. *Proc. Natl. Acad. Sci. USA*, 112:6200–6205, 2015.
- [4] H.C. Astley, J.R. Mendelson, J. Dai, C. Gong, B. Chong, J.M. Rieser, P.E. Schiebel, S.S. Sharpe, R.L. Hatton, H. Choset, and D.I. Goldman. Surprising simplicities and syntheses in limbless self-propulsion in sand. *J. Exp. Biol.*, 223:103564, 2020.
- [5] J.E. Avron, O. Gat, and O.Kenneth. Optimal swimming at low reynolds numbers. *Phys. Rev. E*, 93:186001, 2004.
- [6] J. Bonet and R.D. Wood. *Non-linear continuum mechanics for finite element analysis*. Cambridge University Press, 1997.
- [7] J.P. Butler, I.M. Tolić-Nørrelykke, B. Fabry, and J.J. Fredberg. Traction field, moments, and strain energy that cells exert on their surroundings. *Amer. J. Physiol. Cell Physiol.*, 282:C595–C605, 2002.
- [8] N. Cohen and J.H. Boyle. Swimming at low reynolds number: a beginners guide to undulatory locomotion. *Cont. Phys.*, 29:103–123, 2010.
- [9] JC del Álamo, R Meili, B Álvarez-González, B Alonso-Latorre, E Bastounis, R Firtel, and JC Lasheras. Three-dimensional quantification of cellular traction forces and mechanosensing of thin substrata by Fourier traction force microscopy. *PLoS ONE*, 8(9):e69850, 2013.
- [10] Y. Ding, S. S. Sharpe, A. Masse, and D. I. Goldman. Mechanics of undulatory swimming in a frictional fluid. *PLOS Comp. Biol.*, 8:e1002810, 2012.
- [11] E.Lauga and T.R. Powers. The hydrodynamics of swimming microorganisms. 72:096601, 2009.
- [12] D. I. Goldman. Colloquium: biophysical principles of undulatory selfpropulsion in granular media. 86:943–958, 2014.
- [13] J. Gray and G. J. Hancock. The propulsion of sea-urchin spermatozoa. *J. Exp. Biol.*, 32:802, 1955.
- [14] R. L. Hatton, Y. Ding, H. Choset, and D. I. Goldman. Geometric visualization of self-propulsion in a complex medium. *Phys. Rev. Letters*, 110(7):078101, 2013.
- [15] D.L. Hu, J. Nirody, T. Scott, and M.J. Shelley. The mechanics of slithering locomotion. *Proc. Natl. Acad. Sci. USA*, 106:10081–10085, 2009.
- [16] J. Korta, D.A. Clark, C.V. Gabel, L. Mahadevan, and A.D.T. Samuel. Mechanosensation and mechanical load modulate the locomotory gait of swimming *C. elegans*. *J. Exp. Biol.*, 210:2383–2389, 2007.
- [17] WR Legant, CK Choi, JS Miller, L Shao, L Gao, E Betzig, and CS Chen. Multidimensional traction force microscopy reveals out-of-plane rotational moments about focal adhesions. *Proc. Natl. Acad. Sci. USA*, 110(3):881–886, 2013.
- [18] R. D. Maladen, Y. Ding, C. Li, and D. I. Goldman. Undulatory swimming in sand: Subsurface locomotion of the sandfish lizard. *Science*, 325:314–318, 2009.
- [19] Z. Peng, Y. Ding, K. Pietrzyk, G.J. Elfring, and O. S. Pak. Propulsion via flexible flapping in granular media. *Phys. Rev. E*, 96:012907, 2017.
- [20] E.M. Purcell. Live at low Reynolds number. *Amer. J. Phys.*, 45(1):3–11, 1977.

- [21] A. Shapere and F. Wilczek. Geometry of self-propulsion at low Reynolds number. *198*:557–685, 1989.
- [22] S. S. Sharpe, S. A. Koehler, R. M. Kuckuk, M. Serrano, P. A. Vela, J. Mendelson, and D. I. Goldman. Locomotor benefits of being a slender and slick sand swimmer. *J. Exp. Biol.*, 218:440–450, 2015.
- [23] G.J. Stephens, B. Johnson-Kerner, W. Bialek, and W.S. Ryu. Dimensionality and dynamics in the behavior of *C. elegans*. *PLOS Comp. Biol.*, 4:e1000028, 2008.
- [24] H.A. Stone and A.D.T. Samuel. Propulsion of microorganisms by surface distortions. *Phys. Rev. Letters*, 77(19):4102–4104, 1996.
- [25] R. Sunyer, V. Conte, J. Escribano, A. Elosegui-Artola, A. Labernadie, L. Valon, D. Navajas, J.M. García-Aznar, J.J. Muñoz, P. Roca-Cusachs, and X. Trepat. Collective cell durotaxis emerges from long-range intercellular force transmission. *Science*, 353(6304):1157–1161, 2016.
- [26] G.I. Taylor. Analysis of the swimming of microscopic organisms. *Proc. Royal Soc. A*, 209:447–611, 1951.
- [27] L. Tesio, V. Rota, C. Chessa, and L. Perucca. The 3d path of body centre of mass during adult human walking on force treadmill. *J. Biomechanics*, 43:938–944, 2010.
- [28] B. D. Texier, A. Ibarra, and F. Melo. Helical locomotion in a granular medium. *Phys. Rev. Letters*, 119(6):068003, 2017.
- [29] J.L. van Leeuwen, C.J. Voesenek, and U.K. Müller. How body torque and Strouhal number change with swimming speed and developmental stage in larval zebrafish. *J. R. Soc. Interface*, 12(110):20150479, 2015.
- [30] G. Xiong and G.V. Lauder. Center of mass motion in swimming fish: effects of speed and-locomotor mode during undulatory propulsion. *Zool.*, 117:269–281, 2014.